

Efficient Real-time Smoke Filtration with 3D LiDAR for Search and Rescue with Autonomous Heterogeneous Robotic Systems

Alexander Kyuroson*, Anton Koval* and George Nikolakopoulos*

*Robotics and Artificial Intelligence Group,

Department of Computer, Electrical and Space Engineering,

Luleå University of Technology, Luleå SE-97187, Sweden

Email: akyuroson@gmail.com

Abstract—Search and Rescue (SAR) missions in harsh and unstructured Sub-Terranean (Sub-T) environments in the presence of aerosol particles have recently become the main focus in the field of robotics. Aerosol particles such as smoke and dust directly affect the performance of any mobile robotic platform due to their reliance on their onboard perception systems for autonomous navigation and localization in Global Navigation Satellite System (GNSS)-denied environments. Although obstacle avoidance and object detection algorithms are robust to the presence of noise to some degree, their performance directly relies on the quality of captured data by onboard sensors such as Light Detection And Ranging (LiDAR) and camera. Thus, this paper proposes a novel modular agnostic filtration pipeline based on intensity and spatial information such as local point density for removal of detected smoke particles from Point Cloud (PCL) prior to its utilization for collision detection. Furthermore, the efficacy of the proposed framework in the presence of smoke during multiple frontier exploration missions is investigated while the experimental results are presented to facilitate comparison with other methodologies and their computational impact. This provides valuable insight to the research community for better utilization of filtration schemes based on available computation resources while considering the safe autonomous navigation of mobile robots.

Index Terms—outlier rejection, aerosol particles, heterogeneous robotic systems

I. INTRODUCTION AND BACKGROUND

In recent years, hybrid-robotic systems with multi-sensor payloads have been deployed in harsh SAR scenarios [1] to not only aid in the exploration of the Perceptually Degraded Environments (PDE)s [2] by inspecting the environmental and structural conditions [3] but also assist rescue workers by increasing their situational awareness to improve rescue efforts while ensuring their safety [4] in such time-critical operations.

Furthermore, such autonomous robotic platforms mainly rely on their onboard perception systems in GNSS-denied environments such as Sub-T and extra-terrestrial sub-surfaces [5] for Simultaneous Localization and Mapping (SLAM). To ensure operational safety in such hazardous environments, a

This work has been partially funded by the European Unions Horizon 2020 Research and Innovation Programme under the Grant Agreement No. 101003591 NEX-GEN SIMS. Corresponding author email: akyuroson@gmail.com

combination of LiDAR and vision-based sensors is utilized to perform pose estimation [6] and collision avoidance [7]. The presence of aerosol particles such as smoke [8] and dust [6] directly affects the performance of these sensors and increases the noise in captured data. In particular, LiDAR sensors are negatively influenced by aerosol particles which cause undesired measurements [9] of the laser beam thereby resulting in occlusions and additional cluttered and noisy points in generated PCLs [10]; see Figure 1.

It must be noted that LiDARs are more prone to such issues in comparison to RADARs [11] due to their inherent beam divergence and short pulse duration [9]. However, due to their performance in poorly-illuminated environments, accurate range measurements and higher spatial resolution [12] compared to RADARs and RGB-D cameras, LiDARs have been deployed on many autonomous robotic platforms [13].

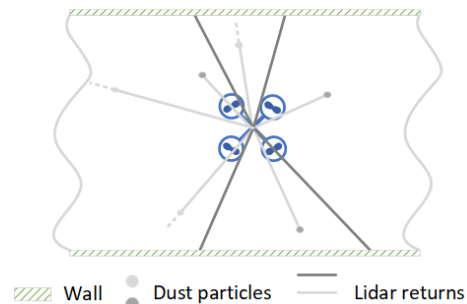
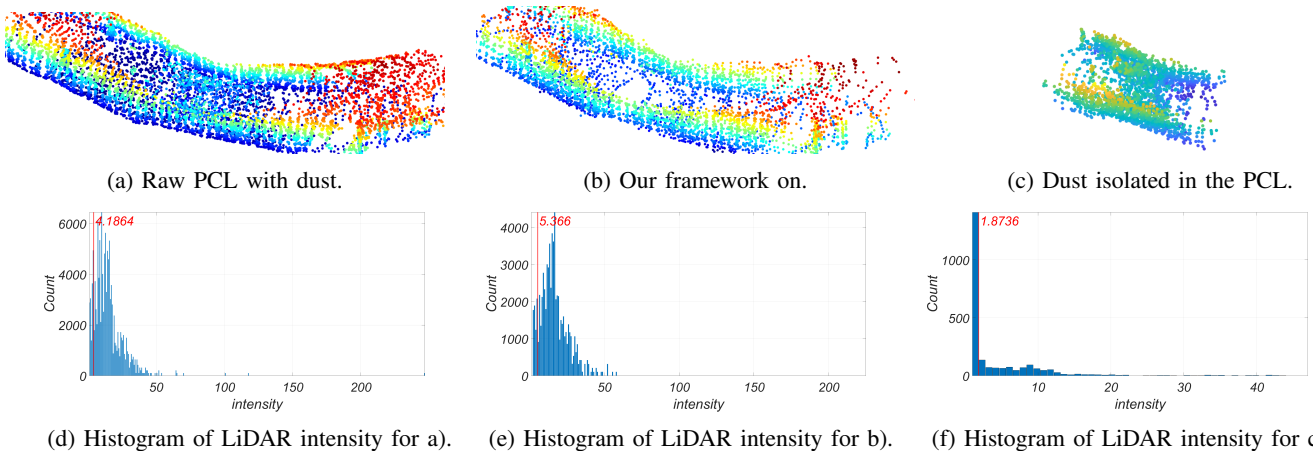


Fig. 1: Behavior of LiDAR in the presence of dust, where the propulsion system of a drone entrains dust particles.

The acquired PCLs are not only used for autonomous navigation of complex environments [13] but also to monitor environmental changes [14], detect artifacts [15], and assess traversability [16]. Therefore, it is vital to identify and remove the points caused by aerosol particles prior to the utilization of data for any other downstream algorithms. To address the aforementioned issues, various PCL filtration methods have been proposed [17]. These methods can be mainly divided into either classical or learning-based approaches [18].

Classical methods such as Radius Outlier Removal (ROR) [19] and Statistical Outlier Removal (SOR) [20] mostly



(d) Histogram of LiDAR intensity for a). (e) Histogram of LiDAR intensity for b). (f) Histogram of LiDAR intensity for c).
 Fig. 2: Test 1. Row 1: Generated PCL map. *Left*, original PCL, *middle*, filtered PCL and isolated dust, *right*. Row 2: Weibull distributions for the PCLs.

rely on spatial information within PCLs to remove outliers based on the local density and distribution of points. This is feasible as points resulting from the aerosol particles have relatively low density compared with their neighboring clusters [21]. However, these methods do not perform reliably in varying density PCLs, where the density of PCLs is proportional to the measured range. Therefore, Dynamic Radius Outlier Removal (DROR) [22] and Dynamic Statistical Outlier Removal (DSOR) [23] are proposed to improve the shortcomings of previous methods by dynamically adjusting the radius based on the range of any given points from the LiDAR to preserve more environmental features [21]. Moreover, by utilizing inherent information such as intensity, aerosol particles can be further identified in LiDAR data [10] as they tend to have low intensity due to the absorption and refraction of most of the beam emitted by LiDAR [24]. Thus, to further improve Low-intensity Outlier Removal (LiOR) [25] and previous dynamic methods, a combination of the DROR and LiOR is proposed [24] to not only address the sparsity issues in the LiDAR data but also improve the $F1$ -score when compared to the previous methods. Compared to DROR, Low-Intensity Dynamic Radius Outlier Removal (LiDROR) has lower time complexity due to the removal of points from PCL at long-range as well as fewer computational operations which resulted from the initial thresholding based on LiOR [25].

Learning-based methods employ both traditional Machine Learning (ML)-based algorithms such as k-Nearest Neighbor (k-NN) [26] and Density-based Spatial Clustering of Applications with Noise (DBSCAN) [27] as well as current deep-learning approaches that are based on various Neural Network (NN) architectures [28] to perform either point- or voxel-wise classification [17]. Additional information such as remittance is also used to further improve the classification of such networks based on the correlation between material type and its reflectance [29]. Furthermore, both the spatial and temporal information is exploited to classify the outliers in PCL by utilizing motion-guided attention blocks [30]. By leveraging the semantic segmentation networks that are well-established, a voxel-wise classifier is capable of segmentation of aerosol

particles in the PCLs [31]. This limits the scope of their usage onboard Micro Aerial Vehicles (MAVs), where due to the payload limitations, only a simple lightweight computing unit can be deployed.

Moreover, other approaches based on Low-Dimensional Manifold Model (LDMM) [32] and Moving Least Squares (MLS) [33] are proposed that exploit the self-similarity of patches from PCL [34]. However, neither of these outlier removal methods can perform reliably in real-time [34]. Therefore, a more robust and computationally efficient framework is required for onboard deployment for autonomous navigation of heterogeneous-robotic systems.

In this paper, a novel modular agnostic filtration framework is proposed to dynamically remove points in LiDAR PCLs resulting from the presence of aerosol particles based on the combination of statistical outlier detection and smoothing filter. Furthermore, the proposed framework is directly coupled to the velocity of the platform and the density of the PCL while performing dynamic down-sampling to ensure low latency and computational complexity.

II. CONTRIBUTIONS

The main contributions of this study are as follows: (a) An online platform-agnostic modular filtration framework for LiDAR data based on both inherent and spatial information from PCL that relies on Dynamic onboard Statistical Cluster Outlier Removal (DoSCOR) approach, which runs solely on CPU. (b) Integration and coupling of the velocity of the robotic platform and time complexity of the algorithm for an adaptive activation of modules for close and long-range filtration. (c) Utilization of Savitzky–Golay (SG) filter to perform outlier rejection via smoothing of the data in $1D$. (d) Evaluation of the proposed framework and its viability for field deployment and utilization in conjunction with collision avoidance method based on the Artificial Potential Field (APF) [13]. (e) Experimental performance evaluation of the proposed approach in Sub-T environments in the presence of aerosol particles.

The remainder of this article is structured as follows. Section III presents a detailed description of the implemented

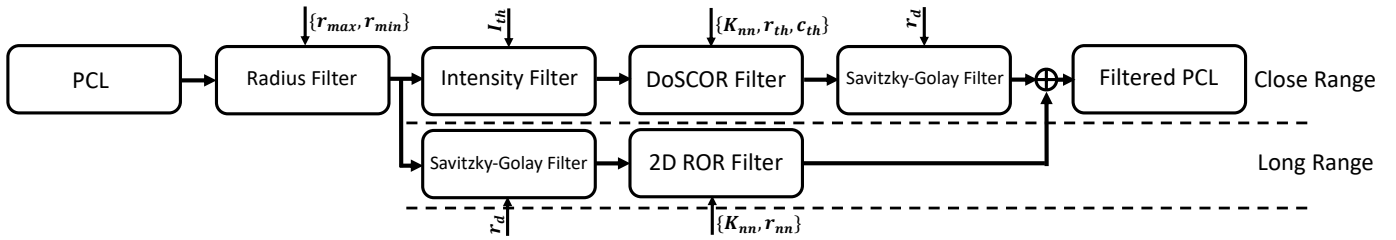


Fig. 3: Overview of the PCL filtration framework.

framework and discuss individual modules of the pipeline and their corresponding functionalities. Furthermore, experimental evaluation of the proposed pipeline and its effect on the obstacle avoidance algorithm is presented in Section IV. Finally, we conclude this article by discussing the achieved results and future work in Section V.

III. METHODOLOGY

In this Section, the proposed modular outlier detection and removal method that is based on the dynamic clustering and SG is presented. The overall proposed pipeline with its subsequent processes is shown in Figure 3. Element-wise pipeline descriptions and their computational impact are further analyzed and presented in this section.

A. Environmental Noise Characterization

As shown in Figure 2, aerosol particles such as smoke and dust in Sub-T environments make an evident impact on SLAM algorithms. The resulting maps of the environment based on the acquired PCLs in such conditions are cluttered and noisy and prevent optimal exploration and detection of survivors in SAR missions. Figure 4 illustrates an example of such environments, where the proposed framework is assessed in the presence of aerosol particles.

As depicted in Figure 1, the behaviors of the LiDAR scans in the presence of aerosol particles such as dust and smoke are directly related to the decomposition of aerosol particles, the LiDAR beam characteristics, and the material properties of the environment where the robot is located [9]. These behaviors can be summarized as no obstruction, full obstruction, partial obstruction, and full loss of LiDAR data [9]. In no obstruction cases, due to the low density of aerosol particles, the LiDAR can penetrate through the particles and detect obstacles. However, this is not feasible when the LiDAR beam is fully absorbed. Therefore, in the presence of high-density aerosol particles, it is feasible to falsely classify such cloud formations as either a part of the environment or obstacles. As such, the combined effect results in noisy and cluttered PCLs with possible occlusions that prevent optimal navigation of the PDEs. Subsequently, other perception algorithms that rely on LiDAR data such as SLAM, object detection, and collision avoidance would be directly affected, and the resulting interference diminishes the operational capabilities of any robotic platform [31].

B. Framework Architecture

The proposed framework solely requires unorganized unlabeled PCLs and their xyz -coordinate values as well as LiDAR

intensity associated with these points. The scan measurements captured by the onboard 3D LiDAR are represented as a PCL in the Cartesian Coordinate System (CCS) and are defined according to Robotic Operating System (ROS) coordinate conventions as x - forward, y - left and z - up. The acquired PCLs tend to have noise induced by small particles that can be easily entrained with airflow from, for instance, a drone propulsion system as shown in Figure 4. Thus, the main objective behind the proposed framework is the filtration of noise induced by these particles in three stages as shown in Figure 3, where at first radius-based filtration in a Spherical Coordinate System (SCS) is applied, next intensity-based filtration in CCS is utilized to remove low-intensity points from PCL, thereafter SG is applied to ranging measurements in SCS to remove outliers and finally 2D ROR filter in Cartesian Coordinate Frame (CCF) is used to ensure that the spatial information of the small objects is preserved.

C. LiDAR Filtration

The LiDAR filtration in this paper is implemented in Python within ROS to enable its integration with other frameworks for online deployment. To ensure real-time performance with low computational complexity and deployment in all possible platforms, the input PCL is divided into close and long-range segments to not only prevent loss of spatial information but also create pseudo attention for regions that are vital for operational safety of the heterogeneous robotic system in Human-swarm Interaction (HSI) setting. As shown in Figure 3, each module requires a set of parameters to operate. Thus, the values and selection criteria of these parameters are provided in Table I.

1) *Radius-based Filtration*: To achieve safe traversal in PDEs, Responsibility-sensitive Safety (RSS) model [35] is used to perform radius-based filtration. This allows overall performance improvement by minimizing the number of points required to be processed for navigation while addressing operational safety concerns. To utilize the RSS model, coordinate system conversion from CCS to SCS is performed. To obtain

TABLE I: Required parameters for the proposed framework.

Parameters	Initial Values	Hyper-parametric Conditions
r_{max}	30 m	$r_{max} = \{\max\{d_{lon}\} d_{lon} \in [10, 100]\}$
r_{min}	5 m	$r_{min} = \{\max\{\tau\} \tau \in [2, 10]\}$
I_{th}	2	$I_{th} = \{Q(p, \alpha, \gamma) \max\{p\} \in [0.1, 0.15]\}$, Eq. 5
r_d	{4, 20} m	$r_d = \{\min\{d\} d \in [r_{min} - 1, r_{max} - 10]\}$
K_{nn}	6	$K_{nn} = \{\min\{k\} k \in [3, 6]\}$
r_{th}	0.45 m	$r_{th} = \{\min\{r\} r \in [0.2, 0.6]\}$
c_{th}	0.4	$c_{th} = \{\min\{c\} c \in [0.1, 0.5]\}$
r_{nn}	0.15 m	$r_{nn} = \{\min\{r_{nn}\} r_{nn} \in [0.1, 0.16]\}$

radial distance, r , inclination, θ , and azimuth, ϕ based on (x, y, z) , axial radius, ρ , is given as $\rho = x^2 + y^2$. Thereafter, r can be defined as $r = \sqrt{\rho + z^2}$ while θ and ϕ are calculated as $\theta = \tan^{-1}\left(\frac{\sqrt{\rho}}{z}\right)$ and $\phi = \tan^{-1}\left(\frac{y}{x}\right)$, respectively. The radius thresholds r_{max} is selected such that it satisfies the following conditions:

$$r_{max} = \max\{d_{lon}\}, \quad (1)$$

where d_{lon} represents the longitudinal safe distances from the center of the robotic platform. The longitudinal safe distance is given by:

$$d_{lon} = v_r \eta + \frac{1}{2} a_{accel} \eta^2 + \frac{(v_r + \eta a_{accel})^2}{2 a_{minbrake}} - \frac{(v_f)^2}{2 a_{maxbrake}}, \quad (2)$$

where a_{accel} , $a_{minbrake}$ and $a_{maxbrake}$ represent the maximum acceleration as well as minimum deceleration of the robot and maximum deceleration of the dynamic obstacle in the environment, respectively. Moreover, v_r is the current velocity of the robot and v_f represents the velocity of the dynamic obstacle. The estimated response time of the dynamic obstacle in a poorly illuminated environment is given by η . Additionally, the minimum radius threshold, r_{min} , is adaptively selected based on the time complexity of the algorithm and environmental complexity such that the filtered close-range PCL contains a maximum of $30k$ points. This is achieved by periodically sampling the number of points in close-range PCL. The sampling frequency of 1 Hz is selected for surveying close-range PCL as abrupt changes in the environment are mission critical and they directly affect the safety of the robot and rescue workers.

2) *Intensity-based Outlier Removal*: Based on the LiDAR intensity analysis in the absence and presence of dust and smoke [10], [25], it has been shown that the intensity of LiDAR data can be used to facilitate filtration of the noise in PCL due to the presence of aerosol particles. Furthermore, the intensity information can be utilized to distinguish and identify the material of various surfaces based on their reflectivity [10]. Due to the scattering and absorption of the LiDAR beam by the particles, the intensity value of aerosol particles in PCL is low and their distribution can be characterized based on Weibull Probability Density Function (PDF) [36]. The PDF of the general Weibull distribution is as follows:

$$P(x, \alpha, \gamma, \mu) = \frac{\gamma}{\alpha} \left(\frac{x-\mu}{\alpha}\right)^{\gamma-1} \exp\left(-\left(\frac{x-\mu}{\alpha}\right)^\gamma\right), \quad (3)$$

where γ , μ , and α represent the shape, the location, and the scale parameter, respectively. Moreover, x and α values are subjected to $x \geq \mu$ and $\alpha > 0$. Given $\mu = 0$, the general Weibull distribution equation can be expressed in its standard two-parameter form and is defined as:

$$P(x, \alpha, \gamma) = \frac{\gamma}{\alpha} \left(\frac{x}{\alpha}\right)^{\gamma-1} \exp\left(-\left(\frac{x}{\alpha}\right)^\gamma\right). \quad (4)$$

As shown in Figure 2 and Table II, the intensity distribution of the noise generated in the PCL due to the presence of the aerosol particles has Weibull distribution. This behavior is observed independent of particle type as well as environmental



Fig. 4: Challenging Sub-T environment for LiDAR sensors.

factors [10]. Therefore, the intensity outlier rejection threshold, I_{th} , has an adaptive nature for a given data stream and is based on the Weibull Quantile Function (QF) [37], which is calculated using the following equation:

$$Q(p, \alpha, \gamma) = \alpha (-\ln(1-p))^{\frac{1}{\gamma}}, \quad (5)$$

where $p \in [0, 1]$ represents the probability value such that the calculated I_{th} has less than or equal probability value, p , as shown in Table I. Moreover, this behavior is observed in row two of Figure 2, in which after the noise removal the intensity threshold has changed.

3) *Dynamic onboard Statistical Cluster Outlier Removal*: The proposed DoSCOR module is based on classical ML clustering method, k-NN and its combination with SOR to enhance its capabilities while addressing the non-uniformity in PCLs. Kd-tree is used to structure the previously filtered 3D LiDAR data prior to performing an initial query ball-search within the radius of 0.05 m to detect the nearest neighbors of each point. This enables the analysis and characterization of individual points based on their spatial properties such as the distribution of neighboring points in PCL to identify and detect aerosol particles. Prior to the calculation of the distance vectors between the neighboring points and the resulting mean, μ , and the standard deviation, σ , initial filtering is performed, where the points with $K_{nn} \leq 6$ neighbors are removed from the PCL. To calculate the global static distant threshold, s_{th} , μ and σ are calculated using the following equations:

$$\mu = \frac{1}{n} \sum_{i=1}^n d_i, \quad (6)$$

$$\sigma = \sqrt{\frac{1}{n-1} \sum_{i=1}^n ((d_i - \mu)^2)}, \quad (7)$$

where n is the number of remaining neighbors for each point $P_i = (x, y, z)$ and d_i is the Euclidean distance measured between point P_i and its neighbors. The global distant threshold can be formulated as $s_{th} = \mu + (\sigma \cdot c_{th})$, where c_{th} is a constant and its value is directly proportional to the density of aerosol particle present in the environment. Given the heterogeneous spatial distribution of points in PCL due to the 3D LiDAR spatial resolution and the limited number of beams, a dynamic threshold, d_{th} , is proposed that can be formulated as $d_{th} = (s_{th} \cdot d_i \cdot r_{th})$, where parameter r_{th} is chosen based on the desired point rejection ratio such that points with high spatial variance are removed.

4) *SG Smoothing and Outlier Removal*: Similar to commonly used approaches in robotics, where Kalman filter or ML

is applied for regression, SG algorithm [38] can be utilized to remove the outliers from LiDAR data via smoothing of PCL based on local least-square polynomial approximation in 1D. Denoting LiDAR range measurements, r , corrupted signal, $g(r)$, with additive noise, ϵ_r , with zero mean and finite variance of σ^2 , the $g(r)$ can be formulated by $g(r) = r + \epsilon_r$ [39]. Based on this assumption, the SG polynomial fitting can be applied to the LiDAR range measurements to remove the noise resulting from the presence of the aerosol particles.

The SG smoothing method can be categorized as a kernel-based filtration due to its utilization of a symmetric sampling window of length, w , to compute and minimize the mean-squared error along the input range $g(r)$. The length of the sampling window is defined as $w = 2m + 1$, where w must be larger than the desired fitted polynomial degree n to satisfy the minimum input constraint [38]. Based on the least-square criterion, the summation of the squared differences between the observed range measurements, r_i , and the estimated polynomial, p_i , can be modeled as a cost function δ_m , using the following equation:

$$\delta_m = \sum_{i=-m}^m (p_i - r_i)^2, \quad (8)$$

where $p_i = \sum_{k=0}^n b_{nk} i^k$. Moreover, the k th coefficient of the polynomial p_i is denoted by b_n and its value can be determined by differentiating δ_m with respect to b_n and minimizing the resulting equation. This leads to the following equality equation:

$$\sum_{k=0}^n \left(\sum_{i=-m}^m b_{nk} i^{k+j} \right) = \sum_{i=-m}^m (i^j r_i), \quad (9)$$

where $j \in [0, n]$ is the index representing the equation number, given that there are $n + 1$ equations. To calculate the coefficient vector b , the previous equality equation can be written in a matrix form as $(\mathbf{A}^T \mathbf{A}) b_n = \mathbf{A}^T r_i$, where b_n can be derived as $b_n = (\mathbf{A}^T \mathbf{A})^{-1} \mathbf{A}^T r_i$, given any sequence of range measurements, r_i , from LiDAR [39]. Furthermore, due to the non-uniformity of PCL, an incremental SG implementation is proposed to not only have varied radius threshold, r_d , for close and long-range LiDAR data but also varied polynomial degree, n , and window size, w , to prevent loss of spatial features by over-smoothing of the PCL. Overall, the larger window size and lower polynomial degree result in a higher degree of filtration [39]. Therefore, to achieve the desired noise removal, the optimal window size, w_{opt} , is calculated as follows:

$$w_{opt} = \left[\frac{2(n+2)((2n+3)!)^2 \sigma^2}{((n+1)!)^2} \frac{1}{\nu_n} \right]^{2n+5}, \quad (10)$$

where $\nu_n = \frac{1}{L} \sum_{l=1}^L (r^{(n+2)})^2$ and L is the maximum number of sampling of the LiDAR data in a period τ [39].

5) *2D Radius Outlier Removal*: To minimize the computational cost associated with ROR and preserve the environmental features [21], the 2D ROR filter is implemented by projecting the previously filtered PCL into XY -plane thereby removing the z -axis spatial information from the PCL prior to construction of the Kd-tree for organizing the 2D PCL. There-

after, a search query based on the radius, r_{nn} , is performed to detect the number of neighboring points prior to filtration. Based on the parameter, K_{nn} , which indicates the minimum number of acceptable neighbors for each point $P_d = (x, y)$ in the 2D PCL, the outlier removal is performed. Finally, the remaining points were merged with the close-range modules to produce the filtered PCL as shown in Figure 3.

IV. RESULTS

In this section, the evaluation of the proposed framework and its viability for deployment in real-world scenarios in PDEs, specifically in Sub-T environment located in Luleå, Sweden, is presented. To ensure the safety of both aerial and terrestrial robotic platforms during field experimentation, their traversal velocity is maintained at approximately 1.2 m/s.

A. System setup

The sensor setup and the heterogeneous robotic system, which consists of an aerial and a terrestrial robot [1], is utilized to evaluate the proposed filtration framework. Furthermore, both platforms were equipped with Intel NUC 10 BXNUC10I5FNKPA2.

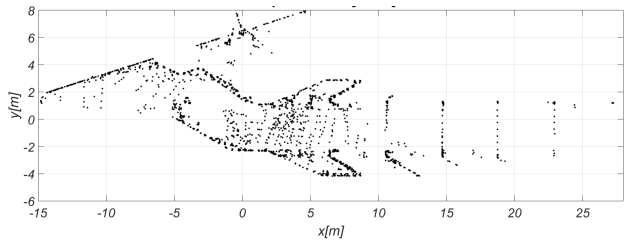
B. Evaluation of SLAM Methods in the PDE

Current State-of-the-Art (SoA) SLAM algorithms such as Direct LiDAR Odometry (DLO) [40] and LiDAR Inertial Odometry via Smoothing and Mapping (LIO-SAM) [41] rely on onboard sensors to achieve localization and mapping of the environment by utilizing the fused LiDAR data in both temporal and spatial domain with Inertial Measurement Unit (IMU) data. To increase the fault tolerance, minimize the impact of noise from acquired LiDAR data, and generate fast and accurate key-frames, these algorithms utilize a combination of voxel-downsampling as well as an adaptive Iterative Closest Point (ICP) scheme based on k-NN and convex hull. However, these strategies are not sufficiently robust against aerosol particles in PDEs as shown in Figure 2a with entrained dust, Figure 5a and Figure 6a, where the generated smoke is falsely identified as an obstacle and is included in the generated map of the Sub-T environment.

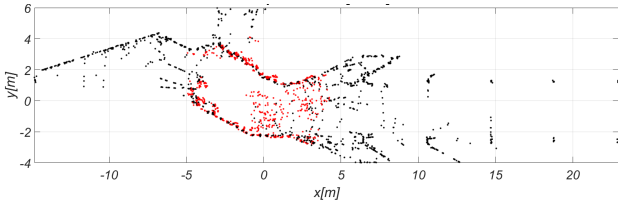
Therefore, to assess the viability of the proposed framework and its impact on the generated map based on DLO, several comparative experiments as illustrated in Figure 5 and Figure 6 are performed in the presence of smoke, where the proposed framework was utilized as a pre-processing step for PCL prior to its utilization in DLO. Figure 5b and Figure 6b highlight the identified aerosol particles which were not included in the generated map when the proposed framework is utilized. By utilizing the proposed framework the entrained dust, Test 1, can be also detected as shown in Figure 2c and removed accordingly, as illustrated in Figure 2b.

C. Evaluation of APF in the PDE

By utilizing the APF method [13] in conjunction with the filtered and unprocessed PCL data stream, the impact of the proposed framework on obstacle detection and avoidance

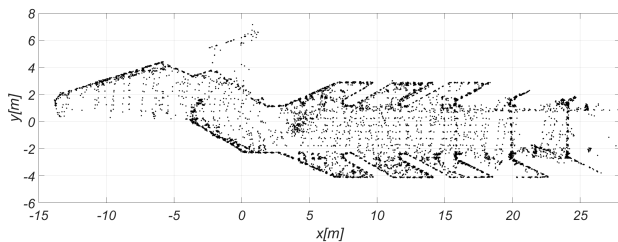


(a) Generated map based on DLO from raw PCL in the presence of smoke.

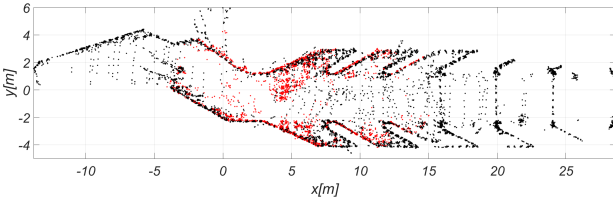


(b) Our framework on. Identified smoke in red, and the environment in black.

Fig. 5: Test 2: DLO map generation with and without our filtration framework.



(a) Generated map based on DLO from raw PCL in the presence of smoke.



(b) Our framework on. Identified smoke in red, and the environment in black.

Fig. 6: Test 3: DLO map generation with and without our filtration framework.

algorithms is studied. As shown in Figure 7, without the utilization of the proposed filtration scheme, the generated reactive forces have a higher variance when compared to their counterparts in Figure 8. Moreover, not only do the magnitude and direction of repulsive forces generated by APF differ in similar conditions in PDE but also in several instances, the APF method could not detect the obstacles within the

TABLE II: Dynamic intensity threshold based on the fitted Weibull distribution for outlier identification from various experiments.

Experiments	Weibull PDF Parameters [α, γ, μ]	Intensity Threshold [I_{th}]	Classes
Test 1	[0.771938, 3.613051, 0.0]	1.873639	51
Test 2	[0.263573, 3.347880, 1.0]	5.276786	28
Test 3	[0.228001, 1.996240, 1.0]	4.614035	57

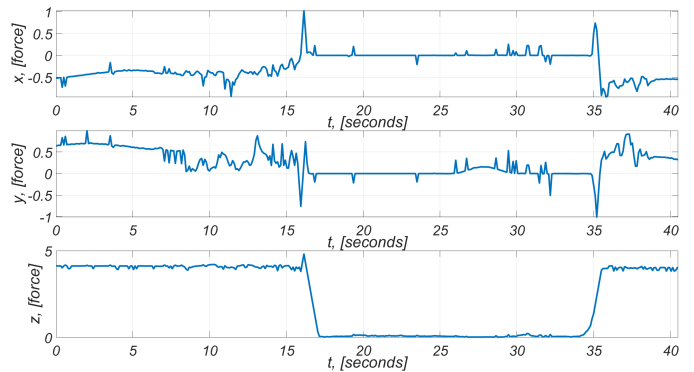


Fig. 7: Potential field forces without the proposed framework.

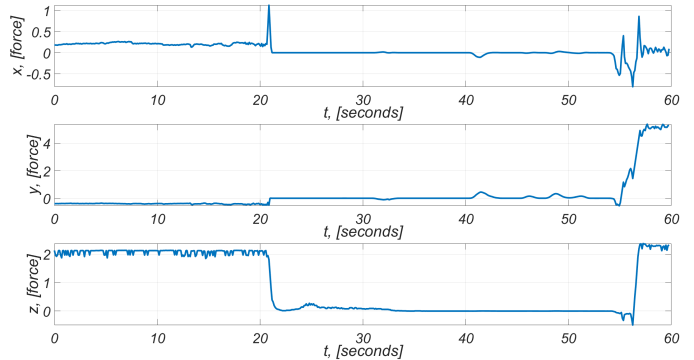


Fig. 8: Potential field forces with the proposed framework.

smoke thereby generating inaccurate forces, which can be observed in y -axis in Figure 7. It must be noted that such false classification will directly affect SAR operations by limiting the scope of autonomous exploration and further hindering object detection algorithms to detect rescue workers and survivors in such harsh environments.

V. CONCLUSIONS

In this paper, an agnostic modular filtration framework for LiDAR data based on both the inherent and spatial information from PCL in harsh and unstructured Sub-T environments with the presence of aerosol particles is presented. The proposed algorithm has demonstrated a solid performance in all experiments having an operational frequency between 10Hz and 20Hz for outlier detection and removal in a scalable pipeline for denser PCLs. Further performance gains can be realized by optimizing clustering methods, implementing dynamic non-uniform regional-based down-sampling of PCL and by implementing the current framework in low-level language like C++. The addition of spatial-temporal coupling can further improve outlier detection and removal by identifying static features thereby isolating noise and dynamic obstacles from the environment. Finally, other unsupervised clustering methods such as HDBSCAN and Local Outlier Factor (LOF) can be further evaluated and their performance, when compared to the current framework, investigated to achieve either better noise isolation or further time complexity improvement of the proposed framework.

REFERENCES

- [1] B. Lindqvist, S. Karlsson, A. Koval, I. Tevetzidis, J. Haluška, C. Kanellakis, A.-a. Agha-mohammadi, and G. Nikolakopoulos, "Multimodality robotic systems: Integrated combined legged-aerial mobility for subterranean search-and-rescue," *Robotics and Autonomous Systems*, vol. 154, p. 104134, 2022.
- [2] S. S. Mansouri, C. Kanellakis, D. Kominiak, and G. Nikolakopoulos, "Deploying mavs for autonomous navigation in dark underground mine environments," *Robotics and Autonomous Systems*, vol. 126, p. 103472, 2020.
- [3] M. Dharmadhikari, H. Nguyen, F. Mascarich, N. Khedekar, and K. Alexis, "Autonomous cave exploration using aerial robots," in *2021 International Conference on Unmanned Aircraft Systems (ICUAS)*. IEEE, 2021, pp. 942–949.
- [4] R. Krzysiak and S. Butail, "Information-based control of robots in search-and-rescue missions with human prior knowledge," *IEEE Transactions on Human-Machine Systems*, vol. 52, no. 1, pp. 52–63, 2022.
- [5] T. N. Titus, J. J. Wynne, M. J. Malaska, A.-a. Agha-Mohammadi, P. B. Buhler, E. C. Alexander, J. W. Ashley, A. Azua-Bustos, P. J. Boston, D. L. Buczowski *et al.*, "A roadmap for planetary caves science and exploration," *Nature Astronomy*, vol. 5, no. 6, pp. 524–525, 2021.
- [6] S. Zhao, H. Zhang, P. Wang, L. Nogueira, and S. Scherer, "Super odometry: IMU-centric LiDAR-Visual-Inertial estimator for challenging environments," in *2021 IEEE/RSJ International Conference on Intelligent Robots and Systems (IROS)*, 2021, pp. 8729–8736.
- [7] B. Lindqvist, S. S. Mansouri, A.-a. Agha-mohammadi, and G. Nikolakopoulos, "Nonlinear MPC for collision avoidance and control of UAVs with dynamic obstacles," *IEEE Robotics and Automation Letters*, vol. 5, no. 4, pp. 6001–6008, 2020.
- [8] C. X. Lu, S. Rosa, P. Zhao, B. Wang, C. Chen, J. A. Stankovic, N. Trigoni, and A. Markham, "See through smoke: robust indoor mapping with low-cost mm-wave radar," in *Proceedings of the 18th International Conference on Mobile Systems, Applications, and Services*, 2020, pp. 14–27.
- [9] T. G. Phillips, N. Guenther, and P. R. McAree, "When the dust settles: The four behaviors of lidar in the presence of fine airborne particulates," *Journal of field robotics*, vol. 34, no. 5, pp. 985–1009, 2017.
- [10] P. Fritsche, S. Kueppers, G. Briese, and B. Wagner, *Fusing LiDAR and Radar Data to Perform SLAM in Harsh Environments*. Cham: Springer International Publishing, 2018, pp. 175–189.
- [11] M. Khader and S. Cherian, "An introduction to automotive lidar," *Texas Instruments*, 2020.
- [12] J. Zhang and S. Singh, "Low-drift and real-time lidar odometry and mapping," *Autonomous Robots*, vol. 41, pp. 401–416, 2017.
- [13] B. Lindqvist, C. Kanellakis, S. S. Mansouri, A. akbar Agha-mohammadi, and G. Nikolakopoulos, "COMPRA: A COMPact reactive autonomy framework for subterranean MAV based search-and-rescue operations," 2021.
- [14] L. Xu, J. Gong, J. Na, Y. Yang, Z. Tan, N. Pfeifer, and S. Zheng, "Shield tunnel convergence diameter detection based on self-driven mobile laser scanning," *Remote Sensing*, vol. 14, no. 3, 2022.
- [15] M. Patel, G. Waibel, S. Khattak, and M. Hutter, "Lidar-guided object search and detection in subterranean environments," 2022.
- [16] L. Zhou, J. Wang, S. Lin, and Z. Chen, "Terrain traversability mapping based on LiDAR and camera fusion," in *2022 8th International Conference on Automation, Robotics and Applications (ICARA)*, 2022, pp. 217–222.
- [17] L. Zhou, G. Sun, Y. Li, W. Li, and Z. Su, "Point cloud denoising review: from classical to deep learning-based approaches," *Graphical Models*, vol. 121, p. 101140, 2022.
- [18] C. Qu, Y. Zhang, K. Huang, S. Wang, and Y. Yang, "Point clouds outlier removal method based on improved mahalanobis and completion," *IEEE Robotics and Automation Letters*, vol. 8, no. 1, pp. 17–24, 2023.
- [19] J. Jia-Jia, W. Xian-Quan, and D. Fa-Jie, "An effective frequency-spatial filter method to restrain the interferences for active sensors gain and phase errors calibration," *IEEE Sensors Journal*, vol. 16, no. 21, pp. 7713–7719, 2016.
- [20] A. Carrilho, M. Galo, and R. C. Dos Santos, "Statistical outlier detection method for airborne lidar data," *International Archives of the Photogrammetry, Remote Sensing & Spatial Information Sciences*, vol. 42, no. 1, 2018.
- [21] M. H. Prio, S. Patel, and G. Koley, "Implementation of dynamic radius outlier removal (DROR) algorithm on lidar point cloud data with arbitrary white noise addition," in *2022 IEEE 95th Vehicular Technology Conference: (VTC2022-Spring)*, 2022, pp. 1–7.
- [22] N. Charron, S. Phillips, and S. L. Waslander, "De-noising of LiDAR point clouds corrupted by snowfall," in *2018 15th Conference on Computer and Robot Vision (CRV)*. IEEE, 2018, pp. 254–261.
- [23] A. Kurup and J. Bos, "Dsor: A scalable statistical filter for removing falling snow from lidar point clouds in severe winter weather," 2021.
- [24] A. Afzalaghaeinaeini, J. Seo, D. Lee, and H. Lee, "Design of dust-filtering algorithms for lidar sensors using intensity and range information in off-road vehicles," *Sensors*, vol. 22, no. 11, 2022.
- [25] J.-I. Park, J. Park, and K.-S. Kim, "Fast and accurate desnowing algorithm for lidar point clouds," *IEEE Access*, vol. 8, pp. 160202–160212, 2020.
- [26] C. Duan, X. Chen, and J. Kovacevic, "Weighted multi-projection: 3d point cloud denoising with tangent planes," in *2018 IEEE Global Conference on Signal and Information Processing (GlobalSIP)*. IEEE, 2018, pp. 725–729.
- [27] K. Zhao, X. Youchun, L. Yongle, and W. Rendong, "Large-scale scattered point-cloud denoising based on VG-DBSCAN algorithm," *Acta Optica Sinica*, vol. 38, 10 2018.
- [28] R. Heinzler, F. Piewak, P. Schindler, and W. Stork, "Cnn-based lidar point cloud de-noising in adverse weather," *IEEE Robotics and Automation Letters*, vol. 5, no. 2, pp. 2514–2521, 2020.
- [29] C. Reymann and S. Lacroix, "Improving lidar point cloud classification using intensities and multiple echoes," in *2015 IEEE/RSJ International Conference on Intelligent Robots and Systems (IROS)*. IEEE, 2015, pp. 5122–5128.
- [30] R. Alexandru Rosu, P. Schütt, J. Quenzel, and S. Behnke, "Latticenet: Fast spatio-temporal point cloud segmentation using permutohedral lattices," *arXiv e-prints*, pp. arXiv–2108, 2021.
- [31] A. Seppänen, R. Ojala, and K. Tammi, "4denoisenet: Adverse weather denoising from adjacent point clouds," *IEEE Robotics and Automation Letters*, vol. 8, no. 1, pp. 456–463, 2023.
- [32] S. Osher, Z. Shi, and W. Zhu, "Low dimensional manifold model for image processing," *SIAM Journal on Imaging Sciences*, vol. 10, no. 4, pp. 1669–1690, 2017.
- [33] G. Guennebaud, M. Germann, and M. Gross, "Dynamic sampling and rendering of algebraic point set surfaces," in *Computer Graphics Forum*, vol. 27, no. 2. Wiley Online Library, 2008, pp. 653–662.
- [34] J. Zeng, G. Cheung, M. Ng, J. Pang, and C. Yang, "3d point cloud denoising using graph laplacian regularization of a low dimensional manifold model," *IEEE Transactions on Image Processing*, vol. 29, pp. 3474–3489, 2020.
- [35] M.-J. Kim, S.-H. Yu, T.-H. Kim, J.-U. Kim, and Y.-M. Kim, "On the development of autonomous vehicle safety distance by an rss model based on a variable focus function camera," *Sensors*, vol. 21, p. 6733, 10 2021.
- [36] P. Helmholz, D. Belton, N. Oliver, J. Hollick, and A. J. Woods, "The influence of the point cloud comparison methods on the verification of point clouds using the batavia reconstruction as a case study," in *Proceedings of the Sixth International Congress for Underwater Archaeology*, 2020, pp. 370–381.
- [37] D. P. Murthy, M. Xie, and R. Jiang, *Weibull models*. John Wiley & Sons, 2004.
- [38] A. Savitzky and M. J. Golay, "Smoothing and differentiation of data by simplified least squares procedures," *Analytical chemistry*, vol. 36, no. 8, pp. 1627–1639, 1964.
- [39] M. Sadeghi, F. Behnia, and R. Amiri, "Window selection of the savitzky-golay filters for signal recovery from noisy measurements," *IEEE Transactions on Instrumentation and Measurement*, vol. 69, no. 8, pp. 5418–5427, 2020.
- [40] K. Chen, B. T. Lopez, A.-a. Agha-mohammadi, and A. Mehta, "Direct lidar odometry: Fast localization with dense point clouds," *IEEE Robotics and Automation Letters*, vol. 7, no. 2, pp. 2000–2007, 2022.
- [41] T. Shan, B. Englot, D. Meyers, W. Wang, C. Ratti, and D. Rus, "LIO-SAM: Tightly-coupled Lidar Inertial Odometry via Smoothing and Mapping," in *IEEE/RSJ International Conference on Intelligent Robots and Systems (IROS)*, 2020.